THE JOURNAL OF BIOLOGICAL CHEMISTRY
Vol. 277, No. 23, Issue of June 7, pp. 20794–20803, 2002
Printed in U.S.A.

Computer Modeling of Three-dimensional Structure of DNA-packaging RNA (pRNA) Monomer, Dimer, and Hexamer of Phi29 DNA Packaging Motor*

Received for publication, December 18, 2001, and in revised form, March 7, 2002
Published, JBC Papers in Press, March 8, 2002, DOI 10.1074/jbc.M112061200

Stephen Hoeprich‡ and Peixuan Guo§

From the Department of Pathobiology, Purdue University, West Lafayette, Indiana 47907

A striking common feature in the maturation of all linear double-stranded DNA viruses is that their lengthy genome is translocated with remarkable velocity into the limited space within a preformed protein shell and packaged into near crystalline density. A DNA-translocating motor, powered by ATP hydrolysis, accomplishes this task, which would otherwise be energetically unfavorable. DNA-packaging RNA, pRNA, forms a hexameric complex to serve as a vital component of the DNA translocating motor of bacterial virus Phi29. The sequential action of six pRNA ensures continual function in the DNA translocation process. The Phi29 motor has been assembled with purified components synthesized by chemical or biotechnological approaches and is able to pump the viral DNA into the protein shell *in vitro*. pRNA dimers are the building blocks of the hexamer. The computer models of the three-dimensional structure of the motor was constructed based on experimental data derived from photoaffinity cross-linking by psoralen, phenphi (*cis*-Rh(1,10-phenanthroline)(9,10-phenanthrenequinone diimine)Cl_2^+), and azidophenacyl; chemical modification and chemical modification interference with dimethyl sulfate, 1-cyclohexyl-3-(2-morpholinoethyl)carbodiimide metho-*p*-toluene sulfonate, and kethoxal; complementary modification; and nuclease probing by single- and double-stranded specific RNases. The shapes of these computer models are very similar to the published pRNA images of cryo-atomic force microscopy. pRNA hexamer docking with the connector crystal structure reveals a very impressive match with the available biochemical, genetic, and physical data.

The amazing diversity in RNA function is attributed to the astonishing variety of RNA species and the flexibility in RNA structure. To elucidate the question of how RNA molecules perform their versatile and novel functions, it is crucial to understand the principles and rules that regulate RNA structure. Because of its complexity and versatility, the criterion in RNA folding remains to be elucidated, and determination of RNA structure is an arduous task.

Double-stranded DNA viruses package their genomic DNA into a preformed protein shell, the procapsid (for reviews, see Refs. 1–3). In the case of Phi29, a bacterial virus that infects *Bacillus subtilis*, translocation of double-stranded DNA into the procapsid requires a virus-encoded RNA (4, 5), called pRNA[1] (for reviews, see Refs. 6, 7 and 19) (Fig. 1). Mg^{2+} induces appropriate folding of pRNA for dimerization (9, 10). Dimers of pRNA bind to the connector (the portal vertex, the unique site where DNA enters the procapsid (11, 12)) and serve as the building blocks for hexamer assembly (9, 13). The pRNA molecules interact intermolecularly via hand-in-hand interaction to form a hexameric complex that is a crucial part of the viral DNA translocation motor (14–17). The pRNA appears to be directly involved in the DNA translocation process, leaving the procapsid after DNA packaging is completed (18). The sequential action of pRNA ensures the continuous function of the motor (18, 19).

Dimerization of RNA has been shown to play a vital role in a variety of biological functions. Dimerization of retrovirus RNAs via kissing loops governs essential steps in retroviral replication (20–24). We have predicted that dimerization of RNA might play other vital roles in cell cycles (25); for example, RNA/RNA interaction via alternating loops has also been reported for *bicoid* mRNA in *Drosophila* embryos (8, 26). We believe that (25) the mechanism of *bicoid* mRNA interaction and translocation might be similar to that of Phi29 pRNA. It is possible that a *bicoid* mRNA may also form hexameric rings to ride, track, or rotate along Staufen protein during its transportation. Indeed, there is evidence that *bicoid* mRNA can form dimers and multimers via RNA loop/loop interactions (8, 26).

The use of computers to model the pRNA three-dimensional structure has been attempted previously (16, 27). At the time of these studies, very little experimental data regarding the three-dimensional structure of the pRNA monomer, dimer, and hexamers were available. Considering the circumstances in building a pRNA three-dimensional computer model based solely on data from partial secondary structure predictions and computer quantification, the aforementioned computer modeling work was laudable. Recently, the Phi29 DNA packaging motor has become the subject of intense scrutiny (12, 15–17, 28, 29). It has been reported (12) that the published partial hexamer model (16) does not match the size of the Phi29 connector,

* This work was supported by National Institutes of Health Grants GM59944 (mainly) and GM60529 (to P. G.). The costs of publication of this article were defrayed in part by the payment of page charges. This article must therefore be hereby marked "*advertisement*" in accordance with 18 U.S.C. Section 1734 solely to indicate this fact.

The atomic coordinates and structure factors (code 1L4R, 1L4Q, 1L4O, and 1L4P) have been deposited in the Protein Data Bank, Research Collaboratory for Structural Bioinformatics, Rutgers University, New Brunswick, NJ (http://www.rcsb.org/).

‡ Supported by a Purdue presidential fellowship.

§ To whom correspondence should be addressed: Purdue Cancer Research Center, B-36 Hansen Life Science Research Bldg., Purdue University, West Lafayette, IN 47907. Tel.: 765-494-7561; Fax: 765-496-1795; E-mail: guop@purdue.edu.

[1] The abbreviations used are: pRNA, DNA-packaging RNA; cp-pRNA, circularly permuted pRNA; cryo-AFM, cryo-atomic force microscopy; AMT, 4′-aminomethyl-4,5′,8-trimethylpsoralen; DMS, dimethyl sulfate; CMCT, 1-cyclohexyl-3-(2-morpholinoethyl)carbodiimide metho-*p*-toluene sulfonate; phenphi, *cis*-Rh(1,10-phenanthroline)(9,10-phenanthrenequinone diimine)Cl_2^+; GMPS, guanosine 5′-monophosphorothioate; PDB, Protein Data Bank.

the structure of which was recently solved by x-ray crystallography. Now that extensive data on pRNA three-dimensional intra- and inter-molecular interaction have become available (9, 10, 27, 32, 36), it is time to construct computer models of the pRNA with the newly available data on structure and distance constraints. In addition, pRNA dimers are the building blocks in hexamer assembly (13), and a computer model of pRNA dimers has not been reported. This report describes the three-dimensional structure of the pRNA monomer, dimer, and hexamer using computer modeling and based on experimental data derived from photoaffinity cross-linking, chemical modification, and chemical modification interference, complementary modification, and nuclease probing by RNases. The models presented here integrate experimental data not previously used to make other models. These more realistic models can then be used to aid in understanding the role of pRNA in Phi29 DNA packaging motor. Comparison of the computer models with the published pRNA images of cryo-AFM reveals high similarity in shape. Indeed, docking of the pRNA hexamer model with the connector crystal structure reveals a very impressive match with the biochemical, genetic, and physical data currently available.

EXPERIMENTAL PROCEDURES

Cross-linking by Psoralen and Phenphi—The construction of pRNAs has been described previously (33). Cross-linking of pRNA with AMT (10, 34) and phenphi was performed as described previously (35).

Cross-linking by Azidophenacyl—GMPS containing circularly permuted pRNA (cp-pRNAs) were prepared by *in vitro* transcription with T7 RNA polymerase in the presence of 40 mM Tris-HCl, pH7.5, 12 mM $MgCl_2$, 2 mM spermidine, 10 mM NaCl, 1 mM ATP, 1 mM CTP, 1 mM UTP, 0.2 mM GTP, [α-^{32}P]GTP, and 8 mM GMPS (Amersham Biosciences) at 37 °C for 4 h (36). Transcripts containing the 5′-terminal phosphate of GMPS were coupled to an azidophenacyl group (36–38) and then exposed to UV light (Phillips, UVB 20W-TL01, 311 nm) for 15–30 min at 0 °C to produce intramolecular cross-links. Under these conditions, no photoagent-independent cross-links were detected (32).

Cross-linking of pRNA dimers was achieved by mixing equimolar amounts of photoagent-containing cp-pRNA I-a′ with a transcomplementary pRNA A-i′ in TMS (50 mM Tris-HCl, pH 7.8, 10 mM $MgCl_2$, 100 mM NaCl). The pRNAs were incubated on ice for 15 min and then exposed to UV light. Primer extension was performed to identify the cross-linking sites (36).

Chemical Modification—RNAs were modified with the chemicals dimethyl sulfate (DMS), 1-cyclohexyl-3-(2-morpholinoethyl)carbodiimide metho-*p*-toluene sulfonate (CMCT), and β-etoxy-α-ketobutyraldehyde (kethoxal) as reported previously (9, 27). The concentration of chemicals was titrated empirically to produce, on the average, one base modification per pRNA molecule as described (9, 27, 39, 40).

Chemical Modification Interference (41–43)—Two pRNAs, 5′/3′ B-a′ and 23/97 A-b′, were used to produce pRNA dimers (25, 32). RNA 23/97 A-b′ is a 75-base RNA that lacks bases 1–23 and 98–120. This RNA has been shown to be competent in dimer formation (13). pRNA 5′/3′ B-a′ was modified by chemicals, and 23/97 A-b′ was not modified. In addition, primers used in reverse transcriptase extension targeted pRNA 5′/3′ B-a′ specifically. This strategy was used to avoid ambiguous primer extension results (32).

The monomer RNA B-a′ was treated with either DMS or CMCT as described (9, 27, 32) and then mixed with unmodified monomer A-b′ to test their competency in dimer formation. After incubation, the reaction mixture was electrophoresed to separate the monomer from dimer. Both the monomer and dimer, after being isolated from the gel, were subjected to primer extension as described (10). If a modified base is involved in dimer formation, pRNA B-a′ carrying this modified base would not be able to form dimers with A-b′ and thus will be present in the fast migrating band representing the monomer in the gel. The concentration of the modifying chemical was titrated so that on the average only one base of each pRNA was modified.

T1 Ribonuclease Probing—10–20 ng of ^{32}P-labeled pRNA (~3000 cpm) in 2 μl of H_2O was mixed with 6 μl of carrier tRNA (1.75 μg/μl) and dialyzed on a 0.025-μm type VS filter membrane (Millipore Corp.) against TBE (89 mM Tris borate, 2 mM EDTA, pH 8.0) for 15 min. Half of the sample was then transferred into an Eppendorf tube, and the other half was dialyzed further on a VS filter membrane against TMS (50 mM Tris, pH 7.8, 100 mM NaCl, 10 mM $MgCl_2$) for 30 min. One μl of T1 ribonuclease (1 unit/μl from the RNA sequencing kit of United States Biochemical) was added to both samples. After 15 min at ambient temperature, the reactions were stopped by adding an equal volume of stop solution (95% formamide, 0.025% xylene, 10 mM EDTA) and loaded onto an 8% sequencing gel. Both T1 ribonuclease and alkaline hydrolysis ladders were generated following the instructions of the RNA sequencing kit (United States Biochemical) (10).

Creation of the Three-dimensional Models—Models of the pRNA monomer, dimer, and hexamer were produced on Silicon Graphics Indigo^2 and Octane computers running IRIX version 6.2 or 6.5, using the programs NAHELIX, MANIP, PRENUC, NUCLIN, and NUCMULT (44, 45). A Silicon Graphics, Inc. Dials Box attached to the computer was used to provide much of the user input to the MANIP program, including zooming in and out, linear movements, and rotations. Using MANIP, one or more selected nucleotides can be moved, rotated, or torqued in bond angles. Nucleotides can be joined or separated.

The modeling was performed based on the following assumptions. 1) Fragments of the molecule were created using the program NAHELIX. All helices are created as a regular A-form double helix, and sequence-dependent distortions of the helix are generally ignored. 2) Internal loops and mismatched bases are constructed by maintaining the integrity of the double helix while optimizing base-pairing and stacking inside the loop, as suggested by other data from crystallography and NMR studies. 3) A general principle for the modeling of RNA hairpin loops has been proposed (46), which involves maximal stacking on the 3′ side of the stem and enough nucleotides stacked on the 5′ side to allow loop closure as found in the loop of tRNA anticodon. 4) Bulges are constructed either protruding from stems, so that there is no helical distortion, or within the helical domain, forcing the helical axis to bend. The energies for stacking are considered to decide whether bulges should be protruding from or within the helical stems (47). 5) Helix untwisting or twisting, helix-helix interactions, triple base interactions (48), pseudoknots, or other higher order structures have been built into the model at constant geometrical distances but allowing certain torsion angle variation. The principle regarding RNA flexibility has been applied to the construction of the $U^{72}U^{73}U^{74}$ bulge at the three-helix junction of pRNA. This three-base bulge has been found to provide flexibility for the appropriate folding of the three-helix junction. Traditional computer algorithms involving the minimization of empirical energy functions have been considered. 6) Distances between atoms can be monitored as their positions are changed. 12 angstroms has been considered as a maximum distance constraint when bases are cross-linked by GMPS/aryl azide. Modified distance geometry and molecular mechanics algorithms have been considered to generate structures consistent with data from cross-linking, chemical modification, and chemical modification interference. A constraint satisfaction algorithm provided by the program is used to refine the structure to take care of some poorly defined regions of pRNA in order to ensure a plausible representation of all atoms. PRENUC and NUCLIN create certain files needed for the refinement process to begin. NUCMULT refines the model by changing distances and angles to be closer to standard values. More refinements give the model more standardized dimensions, if the user originally makes the model with distances and angles that do not deviate too much from commonly accepted values.

RESULTS AND DISCUSSIONS

Previous work has identified the intermolecular interaction between the right-hand loop (the loop closest to the 5′ terminus of the pRNA) of one RNA molecule and the left-hand loop (the loop closest to the 3′ terminus of the pRNA) of another pRNA molecule (15–17). This intermolecular interaction between the loops for the formation of a hexamer is referred to as a "hand-in-hand" interaction (25). In addition, the pRNA dimer has been shown to be the building block for the formation of the hexameric complex (13). A model for the pathway of hexamer formation has been proposed (13).

The goal of modeling pRNA is to organize collections of structural data from cross-linking, chemical, or ribonuclease probing, cryo-AFM, and other genetic data into a three-dimensional form. Because a large number of structural constraints are available, computer programs can successfully construct three-dimensional structures.

Computer models of the pRNA monomer, dimer, and hexamer and the hexamer-connector complex are presented (Fig. 2, *A–D*,

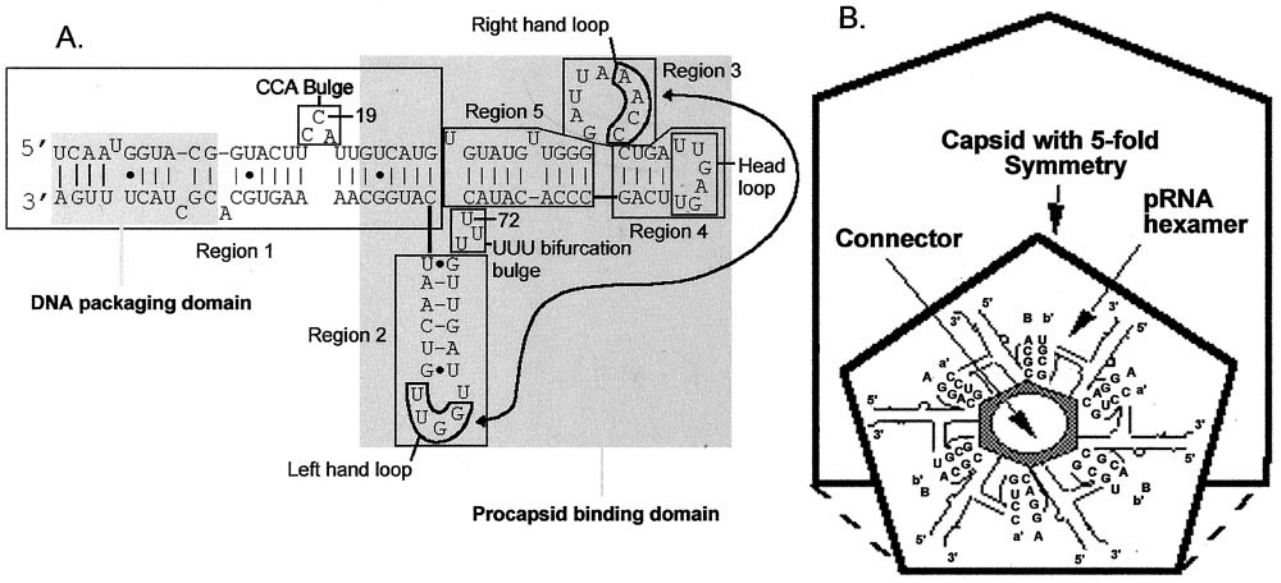

FIG. 1. **Secondary structure of pRNA and procapsid-hexamer complex.** *A*, diagram showing the predicted pRNA secondary structure. The right- and left-hand loops, the head loop, the $U^{72}U^{73}U^{74}$ bulge, and the $C^{18}C^{19}A^{20}$ bulge are *boxed*. The DNA packaging domain (5′/3′ ends) and the procapsid binding domain (the larger area) are *shaded*. The *curved line* (*double-headed arrow*) points to the two interacting loops. *B*, diagram showing hand-in-hand interaction between six pRNA monomers to form a hexamer. The hexamer is shown to bind to the connector (*hashed hexagon*) on the procapsid.

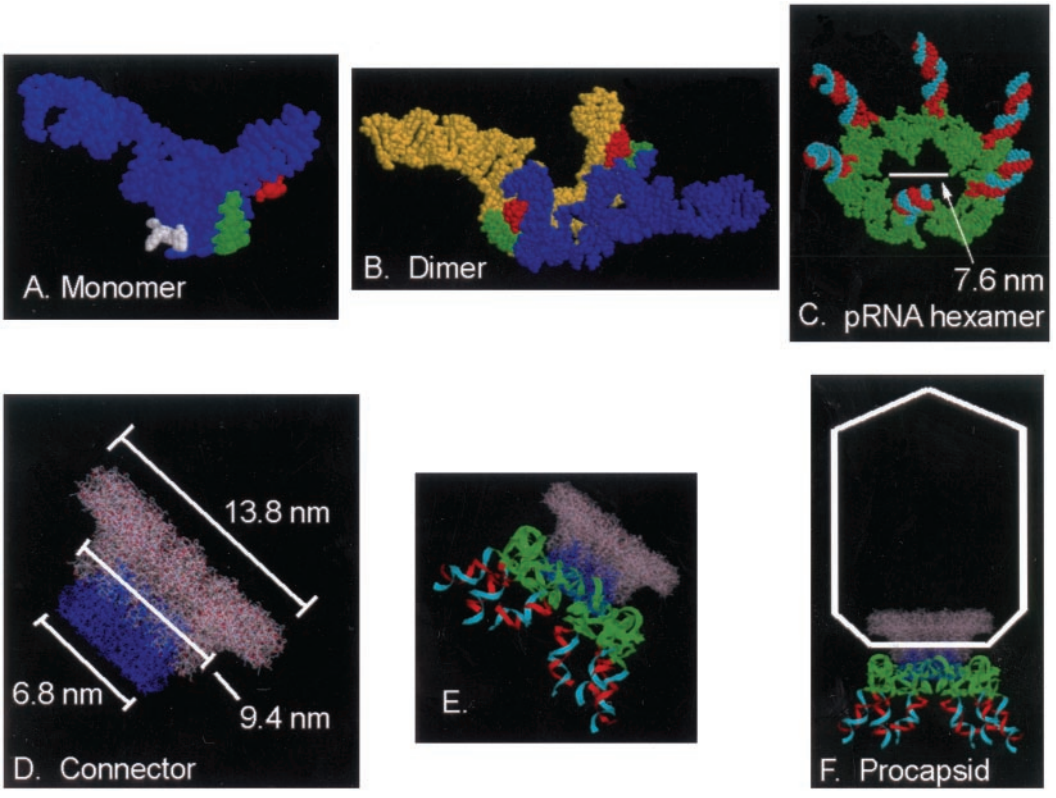

FIG. 2. **Computer models showing the monomer, dimer, hexamer, and connector-pRNA complex.** *A*, The monomer model in space-fill format showing the $U^{72}U^{73}U^{74}$ bulge (*white*) and the right-hand (*red*) and left-hand (*green*) loops. *B*, the dimer model in space-fill format with one unit in *blue* and the other unit in *yellow*. The right- and left-hand loops are *highlighted* in *red* and *green*, respectively. *C*, hexamer model in *space-fill* format showing the procapsid binding domain in *green* and the DNA translocating domain in *red* (5′-end) and *cyan* (3′-end). The DNA translocating domain of the 5′/3′-paired region points *upward*. *D*, the crystal structure of the connector (12) in *wire-frame* format. The RNA recognition motif (19, 31) is colored *blue*. *E*, docking of the pRNA hexamer to the RNA binding domain (RNA recognition motif) of the connector. The connector binding domain is shown in *green* and the DNA translocating domain in *red* and *cyan*. *F*, illustration of the pRNA hexamer-connector complex as part of Phi29.

respectively). The pRNA molecule contains five primary regions (Fig. 1*A*). The first region is the 5′/3′ helix that includes bases 1–28 and 92–117. The second region is the left-hand stem loop incorporating bases 75–91. The third region is made of bases 40–44 and the right-hand loop, composed of bases 45–48. The fourth region is the head-stem loop made of bases 49–62. Bases 30–39 and 71–63 comprise the fifth region, which is the helix between the three-helix junction point and the right-hand loop.

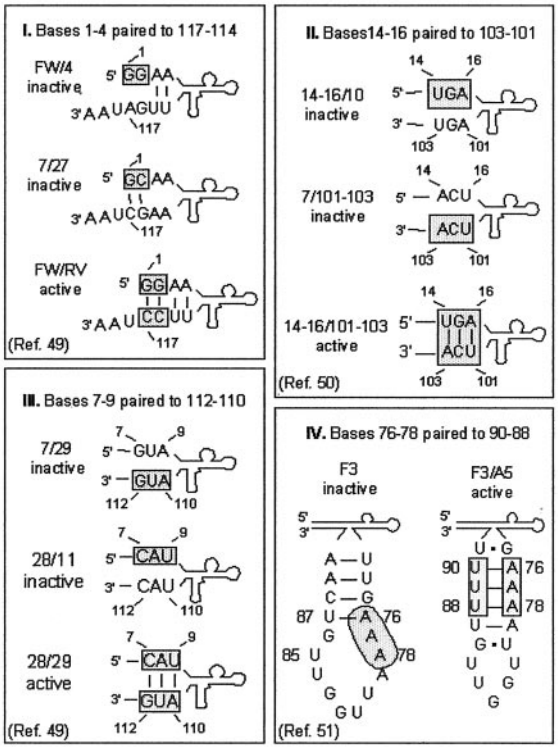

FIG. 3. **Activity (plaque-forming unit (pfu)/ml) of pRNAs by complementary modification (49–51).** Complementary modification verifies predicted secondary structure by comparing the activity or lack of activity to the wild-type sequence.

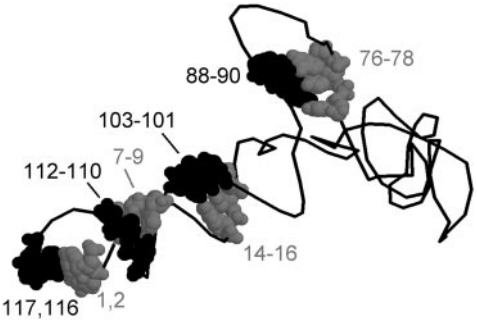

FIG. 4. **Computer model of pRNA monomer to illustrate the results of complementary modification.** Bases mutated in the complementary modification studies are shown in space-filled mode in the three-dimensional model. If the secondary site complementary mutation could restore the pRNA activity, these bases are presented as a helical stretch. The model shows that bases 1 and 2 are paired with bases 117 and 116, bases 7–9 are paired with 112–110, bases 14–16 are paired with 103–101, and bases 76–78 are paired with 90–88.

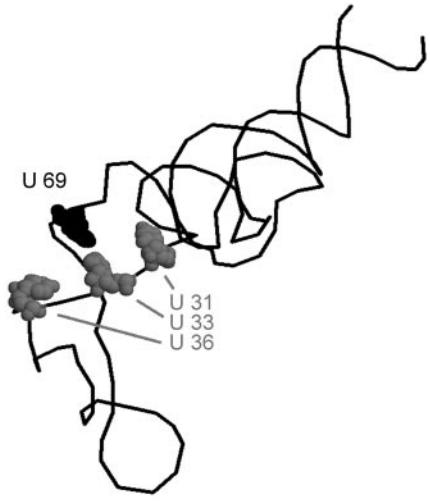

FIG. 5. **Computer model of pRNA monomer to illustrate the results of intramolecular psoralen photoaffinity cross-linking.** The model reflects the experimental data showing that U^{69} (*black*) cross-links to U^{31} and $U^{33}U^{36}$ (*gray*).

Hand-in-hand base-pairing among six monomers forms a hexamer bound to a Phi29 procapsid. The justification for the modeling is described below.

Data to Justify the Construction of the Monomer Model (PDB Code 1L4R)

Complementary Modification Revealed That the 5′ and 3′ Ends of the pRNA Exist as a Helix—Complementary modification was used to confirm the presence of helical regions within the pRNA secondary structure (49–51) predicted by a computer program (52). An extensive series of helix disruptions by base substitutions virtually always resulted in the loss of DNA packaging activity. The inactive pRNAs in this category include pRNA FW/4, pRNA 14–16/10 and 7/101–103, 7/29 and 28/21, and pRNA F3 (Fig. 3). Additional mutations that restored the predicted base-pairing rescued pRNA activity; for example, pRNA FW/RV, pRNA 14–16/101–103, pRNA 28/29, and pRNA F3/A5, with compensatory mutations are all active in Phi29 DNA packaging. The secondary site suppression confirmed that these regions indeed are helical. The computer model of the pRNA monomer supports these data by showing that bases 1 and 2 are paired with bases 117 and 116; bases 7–9 are paired with bases 112–110; bases 14–16 are paired with bases 103–101; and bases 76–78 are paired with bases 90–88. The complementary modification data was incorporated into the three-dimensional monomer model (Fig. 4).

Psoralen Cross-linking Shows That U^{69} is in close proximity to U^{31}, U^{33}, and U^{36}—Psoralen is a photoactive probe for pRNA structure (10) that intercalates into RNA helices. After irradiation with 320–400-nm light, uridines that are in close proximity (helix or pseudoknot) are linked covalently (34, 53, 54). The sites of cross-links can be determined by primer extension (10) and/or mung bean nuclease treatment (55). The psoralen derivative, AMT, was selected for this study because of its solubility (10). Cross-linking with AMT revealed that in the absence of Mg^{2+}, U^{69} is cross-linked to U^{31}, U^{33}, and U^{36}. Although our model was created assuming that Mg^{2+} is present, our computer model of pRNA monomer still provides useful information by showing that U^{69} is not distant from U^{31}, U^{33}, and U^{36} (Fig. 5).

Photoaffinity Cross-linking with Phenphi Showed That Base G^{75} Is in Close Proximity to G^{28} and G^{30}—Phenphi was used to cross-link pRNA (35). UV light was used to activate phenphi, which then formed covalent bonds between guanosine bases. Primer extension was performed, and the reaction was electrophoresed to determine cross-linking sites. Stops in primer extension reactions were observed at U^{29}, U^{31}, and U^{76}, corresponding to cross-links to bases G^{28}, G^{30}, and G^{75}, respectively. The monomer model supports this data by showing that G^{75} is proximate to G^{28} and G^{30} (Fig. 6).

Photoaffinity Cross-linking with Azidophenacyl Showed That Base G^{75} Is in Close Proximity to Bases 26–30, Whereas G^{78} Is Close to U^{31} and G^{108} Is Close to Bases 10 and 11—Circular permutation allows the creation of new 5′/3′ termini of pRNA while maintaining correct folding (37, 50, 56, 57), permitting the labeling of any specific internal base by radioactive or photoaffinity agents. Cross-linking was accomplished by attaching the photosensitive agent azidophenacyl to the new 5′

terminus of the cp-pRNA by the use of GMPS as the first nucleotide incorporated in *in vitro* transcription and coupling with azidophenacyl bromide (32, 36). Three nucleotides were selected as new 5′ termini for labeling with azidophenacyl. One of the new 5′ termini, G^{108}, is located within the helix necessary for DNA packaging, whereas two of the other sites, G^{75} and G^{78}, are located within interior sequences involved in procapsid binding. The particular nucleotides that cross-linked to the new termini of the cp-pRNAs labeled with azidophenacyl were determined by primer extension after UV cross-linking. Extension products from cross-linked cp-pRNA were compared with that from non-cross-linked cp-pRNA to identify individual cross-linked nucleotides. It was found that G^{108} was cross-linked to C^{10} and G^{11}; base G^{75} was cross-linked to A^{26}, U^{27}, G^{28}, U^{29}, and G^{30}; and G^{78} was cross-linked to U^{31} (36). The azidophenacyl group is only 9 Å, but experimental data have demonstrated that the cross-linking group can reach distances of 12 Å.[2] The data suggest that G^{108} is close to C^{10} and G^{11}, G^{75} is close to bases 26–30, and G^{78} is close to U^{31}, as is reflected in the model shown in Fig. 7.

Chemical Modification Showed That the Sequence $C^{18}C^{19}A^{20}$ Forms a Loop Extended above the Surface of the pRNA—Three different chemical probes were utilized to probe the structure of Phi29 pRNA. The chemicals modify atoms in unpaired bases that, if paired instead, are involved in Watson-Crick base-pairing. DMS methylates N1 of adenine and N3 of cytosine (39). CMCT reacts with guanines at N1 and uridines at N3 (39). Kethoxal reacts with guanines at N1 and N2 (39). Base modifications were detected by reverse transcriptase primer extension (39, 40). The samples were subsequently electrophoresed on sequencing gels to determine stops in the extended primers. Stops occur one base prior to modified bases.

Chemical probing of pRNA revealed a large area of protection. However, the three-base bulge $C^{18}C^{19}A^{20}$ (Fig. 8) was accessible to chemicals in monomeric and dimeric as well as procapsid-bound pRNA (9, 27). A pRNA with three bases, 3′-GGU-5′, inserted between A^{99} and A^{100} to pair with the bases $C^{18}C^{19}A^{20}$ in the bulge generates the pRNA 7/GGU (50). This pRNA was fully competent to form dimers and bind procapsids; however its activity in DNA packaging and virion assembly was completely lost (50). A pRNA with a deletion of all three

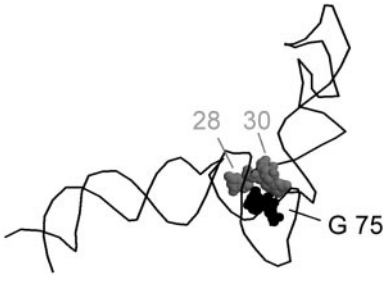

FIG. 6. **Computer model of pRNA monomer to illustrate the results of intramolecular phenphi photoaffinity cross-linking.** The model reflects the experimental data showing that G^{75} (*black*) cross-links to G^{28} and G^{30} (*gray*).

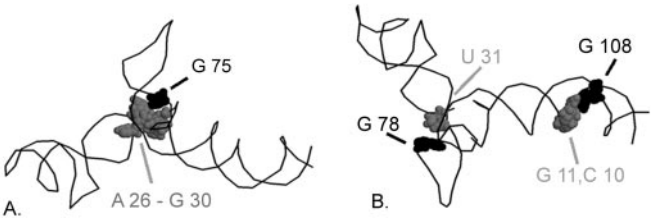

FIG. 7. **Computer model of pRNA monomer to illustrate the results of intramolecular azidophenacyl photoaffinity cross-linking.** *A*, G^{75} (*black*) cross-links to A^{26}, U^{27}, G^{28}, U^{29}, and G^{30} (*gray*). *B*, G 78 (*black*) cross-links to U^{31} (*gray*), and G^{108} (*black*) cross-links to C^{10} and G^{11} (*gray*).

[2] Norman Pace, personal communication.

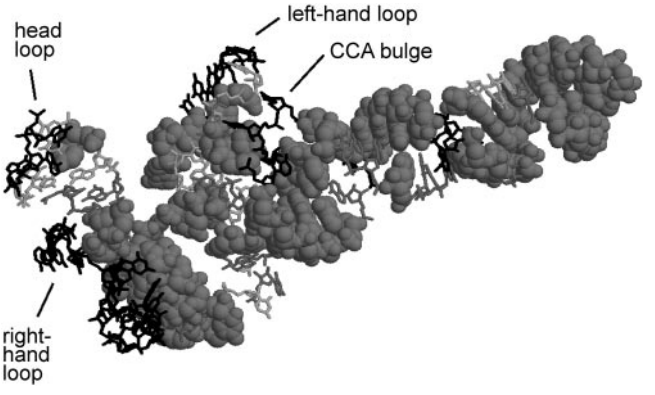

FIG. 9. **Computer model of pRNA monomer to illustrate the results of chemical modification in the presence of Mg^{2+}.** Heavily modified bases, moderately modified bases, and lightly modified bases are shown as *black sticks*, *gray sticks*, and *light gray sticks*, respectively. Note that the single-stranded right-hand loop, head loop, left-hand loop, and the CCA bulge are shown as *black sticks*, indicating a strong modification.

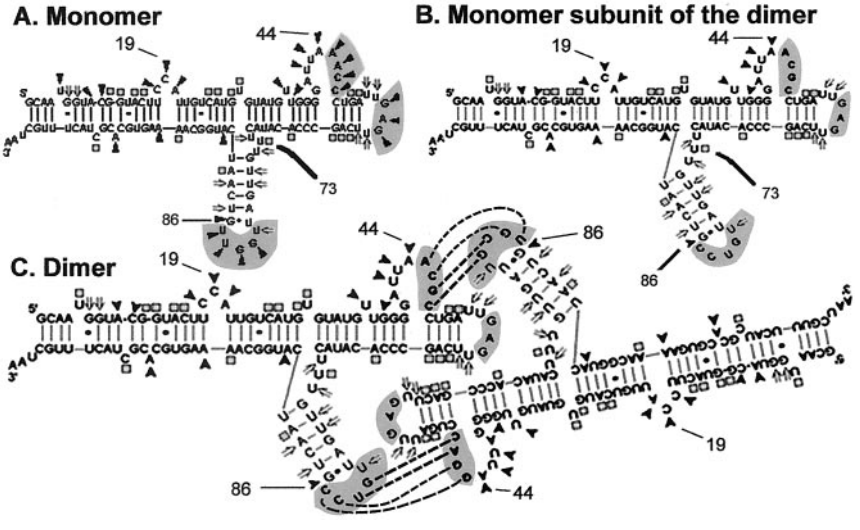

FIG. 8. **Data on comparison of chemical modification pattern of monomer (*A*) and dimer (*B*) (9) for computer modeling.** Each *black arrowhead*, *gray square*, and *double-lined arrow* indicates a strong, moderate, and weak modification, respectively. *C* is portrays the formation of dimer. The four-base-paired sequences (45–48/85–82, *gray boxes*) were modified in monomer but were protected from chemical modification in dimer.

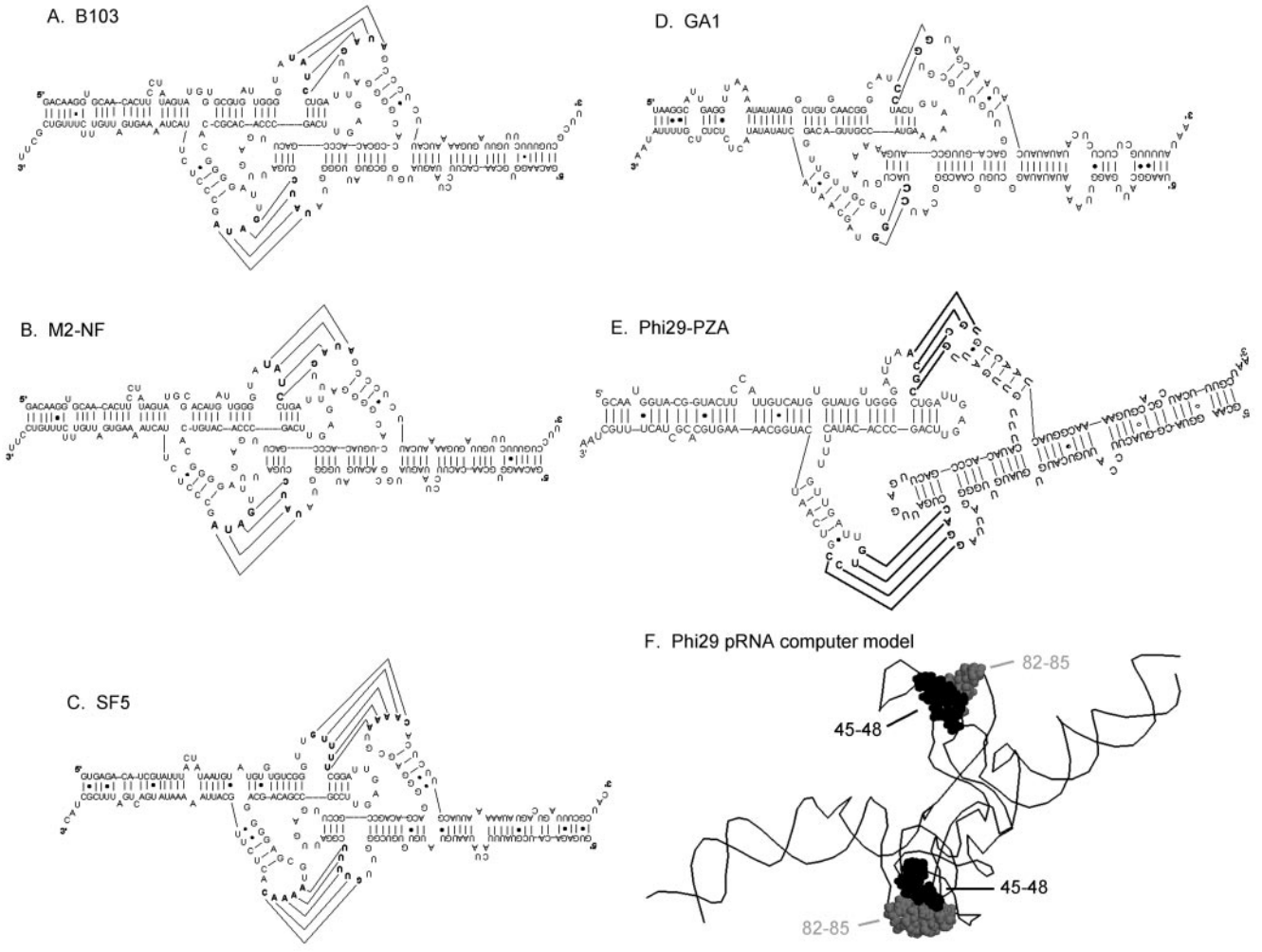

FIG. 10. **Phylogenetic analysis of pRNA.** Phylogenetic analysis of pRNAs from *B. subtilis* phages SF5, B103 (59), Phi29, PZA, M2, NF, and GA1 (60) shows very low sequence identity and few conserved bases, but their predicted secondary structures resemble each other (25, 52). All seven pRNAs of these phages contain both the right and left loops with complementary sequences. The dimer model of Phi29 pRNA (*F*) is in concordance with the data of phylogenetic analysis concerning intermolecular loop/loop interaction in dimer formation. The bases shown in *black space-fill* format (bases 45–48) and *gray* and *black space-fill* format (base 85–82) represent the right- and left-hand loop, respectively.

bases of the CCA bulge (58) exhibited the same biological activity as pRNA 7/GGU concerning procapsid binding, DNA packaging, and virion assembly. The results suggest that CCA, although not involved in procapsid binding, is present on the surface of the pRNA as a bulge to interact with other DNA packaging components (27).

Chemical Modification Reveals Unpaired Bases in Loops and Bulges—As already noted, chemical modification revealed that bases $C^{18}C^{19}A^{20}$ were modified by chemicals and confirmed that these three bases exist as a three-base bulge. Additionally, bases 18–20, 42–48, 55–57, and 82–86 are all strongly modified by chemicals. The monomer model supports these results by showing that all of these bases are present in the model as a single-stranded loop or as bulges (Fig. 9). Phylogenetic analysis of similar RNA from five different phages concurred with these results by showing that all of these bulges are present in similar regions of all five RNA molecules (Fig. 10). All five predicted single-base bulges (50, 51) in Phi29 pRNA are also modified fairly strongly, as are bases A^9, C^{10}, U^{36}, A^{93}, and A^{100}. The monomer model concurs with these data by showing that all of these bases are either present in the model as bulges or are adjacent to or facing a bulge in the complementary strand.

The UUU Presented as a Bulge at the Three-way Junction Provides Flexibility in Folding and Serves as a Hinge for the Twisting of the Lower Stem Loop—Nucleotides $U^{72}U^{73}U^{74}$ were presented in the model as a bulge located at the pRNA three helix junction (Fig. 11). The basis for such construction in the model is that mutation studies showing that deletion of these

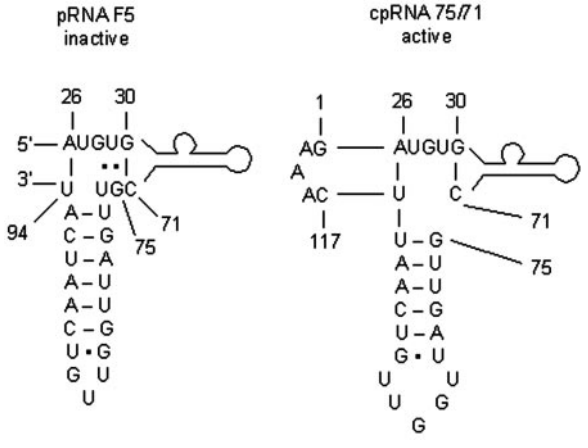

FIG. 11. **$U^{72}U^{73}U^{74}$ region provides flexibility to pRNA.** In pRNA F5, the native 5′/3′ ends have been kept, and U^{72}, U^{73}, and U^{74} have been deleted, resulting in an inactive pRNA (51). In cp-pRNA, the native 5′/3′ ends have been joined by an AAA sequence, and U^{72}, U^{73}, and U^{74} have been deleted to make new 5′/3′ ends, resulting in an active pRNA molecule (50).

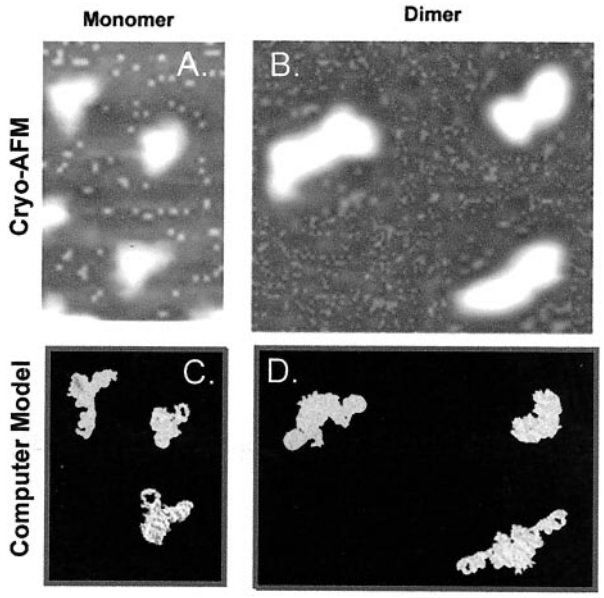

FIG. 12. **Comparison of cryo-AFM images (*A* and *B*) (9, 13, 32) with computer models (*C* and *D*).** The direct observations of the monomer (*A*) and dimer (*B*) by cryo-AFM are compared with the three-dimensional structures of the monomer (*C*) and dimer (*D*) observed from different viewpoint. The illumination in the cryo-AFM images indicates the thickness and height of the images but does not reflect the atom density observed end-on. The *brighter* or *whiter* the illumination, the taller the surface is in the image. The *darker* the illumination, the lower the surface is in the image. Dimers were about twice the length of monomers. The models of the monomer in *C* and the dimer in *D* have been tuned from different angles and aligned with the AFM images.

three nucleotides abolishes the activity of the mutant pRNA F5 with native 5′/3′ ends (51). However, a circularly permuted pRNA, 75/71, that had a deletion of these three nucleotides but had new 5′ and 3′ ends located at bases 75 and 71, respectively, was fully active in *in vitro* Phi29 assembly (50) (Fig. 11), suggesting that the UUU bulge in this area provides flexibility to the pRNA. In pRNA F5 with normal 5′ and 3′ ends, deletion of the UUU bulge eliminated the flexibility in folding of the three-way junction, and therefore the mutant was misfolded. In cp-pRNA 71/75, this flexibility was compensated for by providing a new opening where the F5 pRNA mutant was missing the UUU bulge (51). It is our belief that the new termini in the area of deletion provided comparable flexibility through discontinuity of the phosphodiester bond as was provided by the hinge-like UUU bulge.

Comparison of Computer Monomer Model with Published Monomer Images of Cryo-AFM—Atomic force microscopy has been used by several investigators to detect images of RNA in a denatured conformation. Ph29 pRNA was utilized as the first attempt to examine the three-dimensional structure of RNA in native conformation by cryo-AFM (9, 13, 32).

Cryo-AFM imaging revealed that the pRNA monomer folded into a check mark (✓)-shaped structure resembling the computer monomer model. The brightness and contrast of the image clearly indicate that the area around the head loop (the elbow of the "✓") is the thickest or tallest (Fig. 12) and strongly agrees with the computer model.

Data to Justify the Construction of Dimer Model (PDB Code 1L4Q)

Studies with pRNA mutants have revealed that two single-stranded loops in the pRNA are involved in inter-RNA interactions to form a pRNA hexamer for Phi29 DNA translocation (14, 15, 16, 18) (for a minireview see Ref. 19). These two loops

TABLE I
Data on loop/loop interactions (15) for hexamer modeling using the common multiples of 2, 3, and 6

Two interlocking pRNAs (common multiple of 2)

mutants	Predicted Hexamer	mutants	Predicted Hexamer
I-i' (wild type)	Active	B-a' (unpaired loop)	Inactive
A-b' (Unpaired loop)	Inactive	(A-b')+(B-a') (Compensatory pair)	Active

Three interlocking pRNAs (common multiple of 3)

mutants	Predicted Hexamer	mutants	Predicted Hexamer
A-b' (Unpaired loop)	Inactive	(A-b') + (B-c') (miss one link)	Inactive
B-c' (Unpaired loop)	Inactive	(A-c') + (C-b') (miss one link)	Inactive
C-a' (Unpaired loop)	Inactive	(A-b') + (B-c') + (C-a') (compensatory trimer)	Active

Six interlocking pRNAs (common multiple of 6)

mutants	Predicted Hexamer
(A-b')+(B-c')+(C-d')+ (D-e')+(E-f')+(F-a')	Active

interact alternately to generate interlocking chains. Stable dimer pRNAs have been isolated and purified and are believed to be the intermediate for hexameric complex formation (9, 13, 16, 25). Thus, it is logical to model the dimer and gain some insight about its structure.

Phylogenetics and Mutation Studies Suggested That Bases 45–48 Were Paired Intermolecularly to Base 85–82—Phylogenetic analysis of pRNAs from *B. subtilis* phages B103 (59), SF5, Phi29, PZA, M2, NF, and GA1 (60) shows very low sequence identity and few conserved bases, and yet the family of pRNAs appears to be very similar in predicted secondary structure (25, 52) (Fig. 10). All seven pRNAs of these phages contain both the right and left loops. Complementary sequences within the two loops were found in each of these pRNAs. The numbers of paired bases were from five (5′-GUUUU/CAAAA-5′) for SF5 to four (5′-AACC/UUGG-5′) for Phi29/PZA and B103 to three

(5′-AUC/UAG-5′) for M2/NF and two (5′-CC/GG-5′) for GA1. A loop/loop interaction has been used as a parameter in modeling the pRNA dimer (Fig. 10*F*).

Genetics Studies by in Vitro Mutagenesis—A series of mutant pRNAs carrying mutated right- and/or left-hand loop sequences were made. To simplify the description, we used uppercase and lowercase letters to represent the right- and left hand-hand loop sequences, respectively, of the pRNA (Table I). The same letter in upper- and lowercase symbolizes a pair of complementary sequences. For example, in pRNA A-a′, the right loop A (5′-GGAC^{48}) and left loop a′ (3′-CCUG^{82}) are complementary, whereas in pRNA A-b′, the four bases of the right loop A are not complementary to the sequence of the left loop b′ (3′-UGCG^{82}).

Determination of loop/loop interactions was accomplished by the mixing of inactive mutant pRNAs, each having interactive complementary loops, with each other to determine the loop/loop interaction (15). All mutant pRNAs that had unpaired right and left loops, such as pRNA A-b′, were inactive in *in vitro* Phi29 assembly when used alone. However, when two inactive pRNAs that were transcomplementary in their right and left loops, for example pRNA A-b′ and B-a′, were mixed in a 1:1 molar ratio, full activity was restored. The observed activity of a mixture of two inactive mutants (Table I) suggests that the number of pRNAs in the DNA packaging complex was a multiple of two and confirmed that the right loop interacted with the left loop in dimer formation. Other combinations of pRNA mutants used in this manner suggested that the number of pRNAs in the DNA packaging complex was also a multiple of three and a multiple of six (Table I).

Intermolecular Cross-linking Data—Circularly permutated pRNA B-a′ was made with an azidophenacyl label on G^{82}. Labeled pRNAs were incubated with pRNA A-b′ that has its left and right loop sequences complementary to the right and left loop, respectively, of pRNA B-a′. After UV-cross-linking, dimers were isolated from gels, and the cross-linking site was identified by primer extension. G^{82} was found to cross-link to G^{39}, G^{40}, A^{41}, C^{49}, G^{62}, C^{63}, and C^{64} (36). The computer dimer model support this finding by showing that G^{82}, G^{39}, G^{40}, A^{41}, C^{49}, G^{62}, C^{63}, and C^{64} are all in close proximity and the distance from G82 to these nucleotides is less than 12 angstroms (Fig. 13).

Chemical Modification of Dimer—Dimers consisting of A-b′ and B-a′ pRNAs were chemically modified. Bases C^{85}, C^{84}, U^{83}, G^{82}, A^{45}, C^{46}, G^{47}, and C^{48} were not found modified in dimers, whereas they were modified in monomers (Fig. 8). Each of these bases is within the right- and left-hand loops, which are involved in inter-pRNA interaction (15, 16). Bases G^{57}, A^{56}, and G^{55} located in the head loop were also protected from chemical modification in dimer. A comparison of the modification patterns of monomers and dimers supported the computer model of dimers showing that all three major loops, the right, left, and head loops, were involved in pRNA/pRNA contact to form dimers because all three of these loops were strongly modified in the monomer but protected from modification in dimers (Fig. 9).

Chemical Modification Interference Distinguished Bases Involved from Bases Not Involved in Dimer Formation—Chemical modification interference was performed to determine which bases were involved in dimer formation (32) (Fig. 14). The monomer RNA B/a′ was treated with either DMS or CMCT and then mixed with the unmodified monomer A/b′ to test the competency of the modified RNA in dimer formation. After incubation, the reaction mixture was electrophoresed to separate monomers and dimers. Both monomers and dimers, after isolation from gels, were subjected to primer extension as in other chemical modifications described above. If the modified base is involved in dimer formation, pRNA B-a′ carrying this modified base would not be able to form dimers with A-b′ and thus will be present in the fast migrating band representing the monomer in the gel. The concentration of the modifying chemical was titrated so that on the average only one base of each pRNA would be modified.

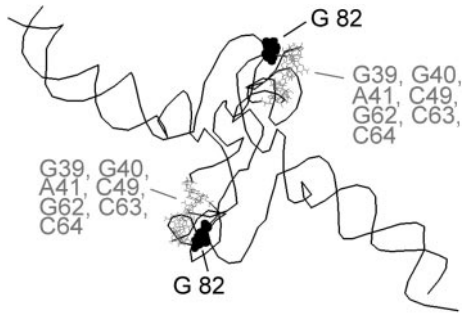

FIG. 13. **Computer model of pRNA dimer to illustrate the results of intermolecular azidophenacyl photoaffinity cross-linking.** The dimer model is in agreement with the empirical data showing that G^{82} (in *black space-fill*) in one pRNA unit approximates G^{39}, G^{40}, A^{41}, C^{49}, G^{62}, C^{63}, and C^{64} (in *gray wire-frame*) of the other pRNA unit.

FIG. 14. **Computer model of pRNA dimer to illustrate the results of chemical modification interference.** Bases that are demonstrated to interfere with dimer formation are shown as *gray*, *space-filled* bases in the pRNA subunits. The dimer model is in agreement with the empirical data showing that these bases are located at the interface of two pRNAs.

Bases 45–49, 52, 54–55, 59–62, 65–66, 68–71, 82–85, and 88–90 showed a very strong involvement in dimer formation as revealed (32) by primer extension showing modification of these bases in RNA isolated from the monomer band. The dimer model (Fig. 14) reveals that each of these bases is located at the interface between two pRNA monomers, coinciding with the data from chemical modification interference.

Comparison of Computer Dimer Model with Published Dimer Images of Cryo-AFM—We have used cryo-AFM to directly visualize purified pRNA dimers (9, 13, 32). The native dimers consisting of pRNAs A-b′ plus B-a′ had an elongated shape. Because the dimer is elongated, it appears that head-to-head contact was involved in dimer formation, resulting in a complex almost twice as long as a monomer. The computer dimer model has a shape that is very similar to the cryo-AFM images (Fig. 12).

Data to Justify the Construction of Hexamer Model (PDB Code 1L4O)

Loop/Loop Interaction to Form a Hexamer—As already noted, dimers are the building blocks of the pRNA hexamer, and the pathway in assembling a hexamer is dimer to tetramer to hexamer (13). It has also been shown that closed dimers, two molecules linked together by the holding of two pairs of hands (intermolecularly base-paired sequences), were active in procapsid binding and DNA packaging, whereas open dimers, formed by the holding of only one pair of hands, are unstable in

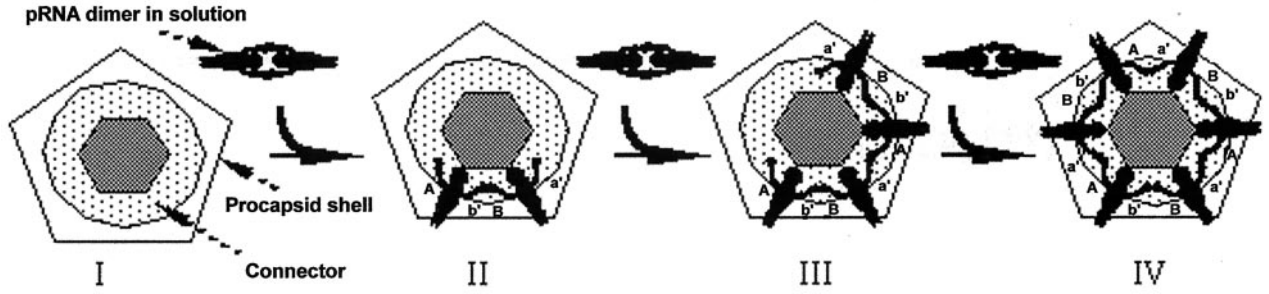

FIG. 15. **A model depicting the assembly of pRNA hexamer from three dimers.** Dimeric pRNA are produced in solution via the hand-in-hand and head-to-head contact (*I*). Binding of the pRNA dimer to the connector, composed of 12 subunits of protein gp10, results in the conformational change of the pRNA dimer, which releases one pair of interacting hands (*II*). The free hand is used to recruit the oncoming dimer via hand-in-hand interaction (*III*). The sequential addition of three dimers resulted in the formation of the pRNA hexamer.

solution (13). Both tandem and fused pRNA dimers with complementary loops designed to form even-numbered rings were active in DNA packaging, whereas those without complementary loops were inactive (13, 16). All of these findings imply that the true pRNA intermediate in hexamer assembly is the closed dimer, with the holding of two pairs of hands, and that the two interacting loops played a key role in recruiting the incoming dimer (Fig. 15). Interestingly, hand-in-hand interaction has also been shown to be the mechanism in pRNA hexamer formation (15, 25). In dimers, each pRNA monomer subunit only holds the hands of one additional pRNA. However, in hexamers each pRNA monomer subunit holds the hands of two additional pRNAs. Thus the hand interaction in dimers and hexamers seems paradoxical, but it can be explained by the finding that the pRNA has a strong tendency to form a circular ring by hand-in-hand contact regardless of whether the final product is a dimer, trimer or hexamer.[3] Therefore, a conformational shift is expected during the transition from dimer to hexamer. We speculate that dimer formation is a prerequisite to generate an appropriate three-dimensional interface for procapsid binding. One of the hands of the dimer would release after binding to the procapsid. The dimer with a released hand is similar to the open (linear) dimer that has been demonstrated to be unstable in solution but is still active in procapsid binding and DNA packaging (25). Such a conformation shift could be the intrinsic nature of such an intriguing RNA that could bear the task of DNA transportation. Indeed, pRNA conformational changes (for a review, see Ref. 19) before and after binding to procapsid have been documented by nuclease probing, cross-linking, and chemical modification (9, 10, 32, 61). Recent studies have provided substantial information regarding the three-dimensional structure of the pRNA (9, 10, 32, 36). To comply with these new data, a new hexamer model was constructed. In this new model, the relative location of the stem loops has been manipulated to fulfill the aforesaid distance constraints (Fig. 2*C*), revealing that the distance between bases G78 and U31 and bases G75 and A26, U27, G28, U29, or G30 are shorter than 12 angstroms (see "Cross-linking of Monomer") (32). Also, within dimers the distance from bases G^{82} to G^{39}, G^{40}, A^{41}, C^{49}, G^{62}, C^{63}, or C^{64} (See "Cross-linking of Dimer") is less than 12 angstroms (36).

Two Functional Domains of the pRNA—Extensive investigation reveals that the pRNA molecule contains two functional domains (Fig. 1*A*). One domain is for connector binding and the other is for DNA translocation (for a review, see Ref. 19). This conclusion comes from the results of: (*a*) base deletion and mutation (33, 49–51, 60), (*b*) ribonuclease probing (10, 61), (*c*) oligo targeting (62, 63), (*d*) competition assays to inhibit phage assembly (14, 63, 64), (*e*) cross-linking to portal protein by UV (65), and (*f*) psoralen cross-linking and primer extension (10). A truncated pRNA comprising bases 28–91 can still be UV cross-linked specifically to the Phi29 connector (65). A 75-base RNA segment comprising bases 23–97 was able to form dimers, interlock into hexamers, compete with full-length pRNA for procapsid binding, and thereby inhibit Phi29 assembly *in vitro* (13). The connector binding domain is located in the central part of the molecule (13, 61, 65), bases 23–97 (Fig. 2, *C*, *E*, and *F*, in *green*), and the DNA translocation domain is located in the 5′/3′ paired ends (33) (Fig. 2, *C*, *E*, and *F*, in *red* and *cyan*).

Protein/RNA cross-linking (65) and connector (portal vertex or gp10) binding assays (5) reveal that pRNA binds to the connector with its procapsid binding domain. Footprinting data reveal that binding of pRNA to procapsid protects bases 26–83 of the pRNA from attack by nucleases (61). Chemical modification revealed that these same areas were inaccessible to chemicals after the pRNA bound procapsid (27) (Fig. 2, *E* and *F*). Our hexamer model complies with the aforementioned data showing that bases 23–97 (Fig. 2, *E* and *F*, in *green*), which is the connector binding domain, interact with the predicted RNA binding domain of the connector (Fig. 2, *E* and *F*, in *blue*), whereas the 5′/3′ paired region (Fig. 2*E*, in *red* and *cyan*), which is the DNA translocation domain, extends away from the connector.

Docking of pRNA Hexamer to Connector (PDB Code 1L4P)—The Phi29 connector contains a wide end and a narrow end. The wide end is embedded in the capsid, and the narrow end is exposed (12, 66, 67). By sequence homology comparison, it was predicted that the connector protein (gp10) contains a conserved RNA recognition motif, residues 148–214, located at the narrow end of the connector that protrudes from the procapsid (11, 31) (for a review, see Ref. 19). Our connector/RNA docking model supports such a prediction by showing that the pRNA hexamer is attached to the RNA recognition motif (Fig. 2*E*, in *blue*), via its connector binding domain (Fig. 2, *C*, *E*, and *F*, in *red* and *cyan*). X-ray crystallography revealed that the connector contains three sections, a narrower section with a diameter of 6.6 nm, a central section with a diameter of 9.4 nm, and a wider section with a diameter of 13.8 nm (12, 67). The hexamer model presented here contains a central channel with a diameter of 7.6 nm that perhaps can sheath onto the narrow end of the connector and would be anchored by the connector central section, which is wider than the central channel of the RNA hexamer (Fig. 2, *E* and *F*).

Acknowledgments—We offer sincere thanks to Dr. Eric Westhof and Benoit Masquida for kind assistance and valuable advice on using the programs NAHELIX, MANIP, PRENUC, NUCLIN, and NUCMULT, Dr. John Turek and Mark Olin for assistance with the Silicon Graphics, Inc. platform at Purdue University, and Dr. Michael Rossmann for consent to use his published crystal structure of the connector. Chaoping Chen, Kyle Garver, Yahya Mat-Arip, Mark Trottier, and Chunlin Zhang also contributed important data to this publication. We

[3] D. Shu and P. Guo, unpublished data.

thank Dr. Zhifeng Shao for collaborative work on the cryo-AFM images of pRNA.

REFERENCES

1. Black, L. W. (1988) in *The Bacteriophages* (Calendar, R., ed) pp. 321–373, Plenum, New York
2. Bazinet, C., and King, J. (1985) *Annu. Rev. Microbiol.* **39,** 109–129
3. Guo, P. (1994) *Semin. Virol.* **5,** 1–3
4. Guo, P., Erickson, S., and Anderson, D. (1987) *Science* **236,** 690–694
5. Guo, P., Bailey, S., Bodley, J. W., and Anderson, D. (1987) *Nucleic Acids Res.* **15,** 7081–7090
6. Anderson, D. L., and Reilly, B. (1993) in *Bacillus subtilis and Other Gram-positive Bacteria: Biochemistry, Physiology, and Molecular Genetics* (Sonenshein, A. L., Hoch, J. A., and Losick, R., eds) pp. 859–867, American Society for Microbiology, Washington, D. C.
7. Guo, P., and Trottier, M. (1994) *Semin. Virol.* **5,** 27–37
8. Wagner, C., Palacios, I., Jaeger, L., St. Johnston, D., Ehresmann, B., Ehresmann, C., and Brunel, C. (2001) *J. Mol. Biol.* **313,** 511–524
9. Trottier, M., Mat-Arip, Y., Zhang, C., Chen, C., Sheng, S., Shao, Z., and Guo, P. (2000) *RNA* **6,** 1257–1266
10. Chen, C., and Guo, P. (1997) *J. Virol.* **71,** 495–500
11. Carazo, J. M., Donate, L. E., Herranz, L., Secilla, J. P., and Carrascosa, J. L. (1986) *J. Mol. Biol.* **192,** 853–867
12. Simpson, A. A., Tao, Y., Leiman, P. G., Badasso, M. O., He, Y., Jardine, P. J., Olson, N. H., Morais, M. C., Grimes, S., Anderson, D. L., Baker, T. S., and Rossmann, M. G. (2000) *Nature* **408,** 745–750
13. Chen, C., Sheng, S., Shao, Z., and Guo, P. (2000) *J. Biol. Chem.* **275,** 17510–17516
14. Trottier, M., and Guo, P. (1997) *J. Virol.* **71,** 487–494
15. Guo, P., Zhang, C., Chen, C., Trottier, M., and Garver, K. (1998) *Mol. Cell* **2,** 149–155
16. Zhang, F., Lemieux, S., Wu, X., St.-Arnaud, S., McMurray, C. T., Major, F., and Anderson, D. (1998) *Mol. Cell* **2,** 141–147
17. Hendrix, R. W. (1998) *Cell* **94,** 147–150
18. Chen, C., and Guo, P. (1997) *J. Virol.* **71,** 3864–3871
19. Guo, P. (2002) *Prog. Nucleic Acids Res. Mol. Biol.* **72,** 415–473
20. Skripkin, E., Paillart, J. C., Marquet, R., Ehresmann, B., and Ehresmann, C. (1994) *Proc. Natl. Acad. Sci. U. S. A.* **91,** 4945–4949
21. Laughrea, M., and Jette, L. (1996) *Biochemistry* **35 No. 5,** 1589–1598
22. Muriaux, D., Rocquigny, H. D., Roques, B. P., and Paoletti, J. (1996) *J. Biol. Chem.* **271,** 33686–33692
23. Greatorex, J. S., Laisse, V., Dokhelar, M. C., and Lever, A. M. L. (1996) *Nucleic Acids Res.* **24,** 2919–2923
24. Clever, J. L., Wong, M. L., and Parslow, T. G. (1996) *J. Virol.* **70,** 5902–5908
25. Chen, C., Zhang, C., and Guo, P. (1999) *RNA* **5,** 805–818
26. Ferrandon, D., Koch, I., Westhof, E., and Nusslein-Volhard, C. (1997) *EMBO J.* **16,** 1751–1758
27. Zhang, C., Trottier, M., Chen, C., and Guo, P. (2001) *Virology* **281,** 281–293
28. Smith, D. E., Tans, S. J., Smith, S. B., Grimes, S., Anderson, D. L., and Bustamante, C. (2001) *Nature* **413,** 748–752
29. Davenport, R. J. (2001) *Science* **291,** 2071–2072
30. Morais, M. C., Tao Y, Olsen, N. H., Grimes, S., Jardine, P. J., Anderson, D., Baker, T. S., and Rossmann, M. G. (2001) *J. Struct. Biol.* **135,** 38–46
31. Grimes, S., and Anderson, D. (1990) *Mol. Biol.* **215,** 559–566
32. Mat-Arip, Y., Garver, K., Chen, C., Sheng, S., Shao, Z., and Guo, P. (2001) *J. Biol. Chem.* **276,** 32575–32584
33. Zhang, C. L., Lee, C.-S., and Guo, P. (1994) *Virology* **201,** 77–85
34. Wassarman, D. A. (1993) *Mol. Biol. Rep.* **17,** 143–151
35. Mohammad, T., Chen, C., Guo, P., and Morrison, H. (1999) *Bioorg. Med. Chem. Lett.* **9,** 1703–1708
36. Garver, K., and Guo, P. (2000) *J. Biol. Chem.* **275,** 2817–2824
37. Nolan, J. M., Burke, D. H., and Pace, N. R. (1993) *Science* **261,** 762–765
38. Harris, M., Nolan, J., Malhotra, A., Brown, J., Harvey, S., and Pace, N. (1994) *EMBO J.* **13,** 3953–3963
39. Ehresmann, C., Baudin, F., Mougel, M., Romby, P., Ebel, J.-P., and Ehresmann, B. (1987) *Nucleic Acids Res.* **15,** 9109–9128
40. Moazed, U., Stern, S., and Noller, H. F. (1986) *J. Mol. Biol.* **187,** 399–416
41. Siebenlist, U., and Gilbert, W. (1980) *Proc. Natl. Acad. Sci. U. S. A.* **77,** 122–126
42. Conway, L., and Wickens, M. (1987) *EMBO J.* **6,** 4177–4184
43. Rymond, B. C., and Rosbash, M. (1988) *Genes Dev.* **2,** 428–439
44. Massire, C., and Westhof, E. (1998) *J. Mol. Graph. Model.* **16,** 197
45. Westhof, E., Dumas, P., and Moras, D. (1985) *J. Mol. Biol.* **184,** 119
46. Haasnoot, C. A. G., Hilbers, C. W., van der Marel, G. A., van Broom, J. H., Singh, U. C., Pattabiraman, N., and Kollman, P. A. (1986) *J. Biomol. Struct. Dyn.* **3,** 843–857
47. Turner, D. H., Sugimoto, N., and Freier, S. M. (1988) *Annu. Rev. Biophys. Chem.* **17,** 167–192
48. Michel, F., Ellington, A. D., Couture, S., and Szostak, J. W. (1990) *Nature* **34,** 578–580
49. Zhang, C. L., Tellinghuisen, T., and Guo, P. (1995) *RNA* **1,** 1041–1050
50. Zhang, C. L., Tellinghuisen, T., and Guo, P. (1997) *RNA* **3,** 315–322
51. Reid, R. J. D., Zhang, F., Benson, S., and Anderson, D. (1994) *J. Biol. Chem.* **269,** 18656–18661
52. Zuker, M. (1989) *Science* **244,** 48–52
53. Tyc, K., and Steitz, J. A. (1992) *Nucleic Acids Res.* **20,** 5375–5382
54. Cimino, G. D., Gamper, H. B., Isaacs, S. T., and Hearst, J. E. (1985) *Annu. Rev. Biochem.* **54,** 1151–1193
55. Hui, C. F., and Cantor, C. R. (1985) *Proc. Natl. Acad. Sci. U. S. A.* **82,** 1381–1385
56. Pan, T., Gutell, R. R., and Uhlenbeck, O. C. (1991) *Science* **254,** 1361–1364
57. Zhang, C. L., Trottier, M., and Guo, P. X. (1995) *Virology* **207,** 442–451
58. Reid, R. J. D., Bodley, J. W., and Anderson, D. (1994) *J. Biol. Chem.* **269,** 9084–9089
59. Pecenkova, T., Benes, V., Paces, J., Vlcek, C., and Paces, V. (1997) *Gene* **199,** 157–163
60. Bailey, S., Wichitwechkarn, J., Johnson, D., Reilly, B., Anderson, D., and Bodley, J. W. (1990) *J. Biol. Chem.* **265,** 22365–22370
61. Reid, R. J. D., Bodley, J. W., and Anderson, D. (1994) *J. Biol. Chem.* **269,** 5157–5162
62. Zhang, C. L., Garver, K., and Guo, P. (1995) *Virology* **211,** 568–576
63. Trottier, M., Garver, K., Zhang, C., and Guo, P. (1997) *Nucleic Acids Symp. Ser.* **36,** 187–189
64. Trottier, M., Zhang, C. L., and Guo, P. (1996) *J. Virol.* **70,** 55–61
65. Garver, K., and Guo, P. (1997) *RNA.* **3,** 1068–1079
66. Jimenez, J., Santisteban, A., Carazo, J. M., and Carrascosa, J. L. (1986) *Science* **232,** 1113–1115
67. Simpson, A. A., Leiman, P. G., Tao, Y., He, Y., Badasso, M. O., Jardine, P. J., Anderson, D. L., and Rossmann, M. G. (2001) *Acta Crystallogr. Sect. D Biol. Crystallogr.* **57,** 1260–1269